Journal of Medicinal Chemistry

Article

Antibacterial Drug Leads: DNA and Enzyme Multi-Targeting

Wei Zhu, Yang Wang, Kai Li, Jian Gao, Chun-Hsiang Huang, Chun-Chi Chen, Tzu-Ping Ko, Yonghui Zhang, Rey-Ting Guo, and Eric Oldfield

J. Med. Chem., **Just Accepted Manuscript** • DOI: 10.1021/jm501449u • Publication Date (Web): 09 Jan 2015

Antibacterial Drug Leads: DNA and Enzyme Multi-Targeting

*Wei Zhu[1], Yang Wang[1], Kai Li[1], Jian Gao[2], Chun-Hsiang Huang[2], Chun-Chi Chen[2], Tzu-Ping Ko[3], Yonghui Zhang[1], Rey-Ting Guo[2] and Eric Oldfield[1,]**

[1] Department of Chemistry, University of Illinois at Urbana-Champaign, 600 South Mathews Avenue, Urbana, Illinois 61801, United States

[2] Industrial Enzymes National Engineering Laboratory, Tianjin Institute of Industrial Biotechnology, Chinese Academy of Sciences, Tianjin 300308, China

[3] Institute of Biological Chemistry, Academia Sinica, Taipei 11529, Taiwan

KEYWORDS

Drug discovery | Protein structure | DNA minor groove binder | Undecaprenyl diphosphate synthase

Abstract

We report the results of an investigation of the activity of a series of amidine and bisamidine compounds against *Staphylococcus aureus* and *Escherichia coli*. The most active compounds bound to an AT-rich DNA dodecamer $(CGCGAATTCGCG)_2$, and using DSC were found to increase the melting transition by up to 24 ˚C. Several compounds also inhibited undecaprenyl diphosphate synthase (UPPS) with IC_{50} values of 100-500 nM and we found good correlations (R^2 = 0.89, *S. aureus*; R^2=0.78, *E. coli)*) between experimental and predicted cell growth inhibition by using DNA ΔT_m and UPPS IC_{50} experimental results together with 1 computed descriptor. We also solved the structures of three bisamidines binding to DNA as well as three UPPS structures. Overall, the results are of general interest in the context of the development of resistance-resistant antibiotics that involve multi-targeting.

Introduction

There is currently a dearth of new antibiotics being introduced with both the United States Centers for Disease Control and Prevention[1] as well as the World Health Organization,[2] and others,[3] warning of the seriousness of the development of widespread antibiotic resistance. The problem is a multi-faceted one with many factors such as use of antibiotics in feedstocks, unnecessary prescriptions, efflux pumps, and drug modifications all contributing to the problem. In addition, of course, random mutations in a target can occur, rendering a drug ineffective. One approach to ameliorate the latter problem is the use of combination therapies and these are the norm for malaria, HIV/AIDS, tuberculosis, as well as cancer therapeutics. While the development of just one new drug is a daunting prospect, the development of two new drugs (with new targets/mechanisms of action) will be even more challenging, hence the interest is new leads that act by multiple-targeting: one drug (drug lead) but two (or more) targets—an approach that can improve efficacy as well as decrease the likelihood of resistance developing. In our lab, we recently used computational screening to try and find novel inhibitors of two anti-bacterial drug targets, farnesyl diphosphate synthase (FPPS)[4,5] and undecaprenyl diphosphate synthase (UPPS),[6] that are involved in bacterial cell wall biosynthesis (and are not the targets of any currently FDA-approved anti-infective drugs). Inhibiting either of these targets would be of interest since it could lead to "resistance reversal" in e.g. meticillin or vancomycin resistant bacteria (in a combination therapy), with UPPS inhibition being of particular interest since humans do not possess a UPPS gene. We found from our *in silico* and *in vitro* work[5,6] that the bisamidine **1** (BPH-1358) was an inhibitor of both FPPS (IC_{50} ~2 μM) as well as UPPS (IC_{50} ~100 nM) and was active against *S. aureus in vitro* (MIC ~250 ng/mL) and *in vivo* (20/20 mice

survived in an i.p. infection model with a MRSA strain) and in addition, **1** (Scheme 1) acted synergistically with meticillin (with a fractional inhibitory concentration index, FICI = 0.25).[6]

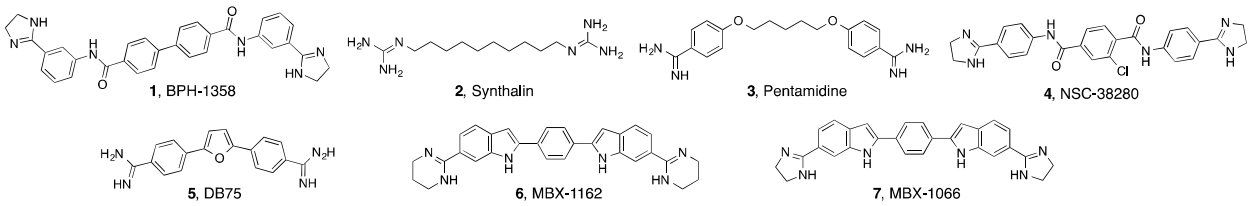

Scheme 1. Structures of bisamidines with anti-infective activity.

1 is, as noted above, a bisamidine (or a diamidine) and somewhat related compounds (derived from synthalin, **2**) have been developed as anti-infectives since ~1937.[7] For example, pentamidine (**3**) has been used against trypanosomatid infections and is still used against *Pneumocystis jirovecii* pneumonia in HIV/AIDS patients. It is, however, a rather toxic compound-despite being on the World Health Organization's List of Essential Medicines. In later work (beginning in 1960), the A. Wander Company[8] developed large numbers of again generally related compounds, bisamidines such as **4**, primarily as anti-leukemia drug leads, but some were also found to have activity against *Trypanosoma brucei*, *T. congolense*, the apicomplexan *Babesia rodaini*, as well as the bacterium *Mycobacterium tuberculosis*.[8] Other bisamidines were later developed and found to have promising activity against several other bacteria[9] and **5** and related compounds (see [10] for a historical perspective) have been in clinical trials for human African trypanosomiasis. In many cases, the mechanism of action (or target) is not completely clear and, interestingly, it has been found with for example **6** and **7**, that DNA synthesis as well as cell wall biosynthesis are targeted (based on macromolecular labeling studies).[11-13] In other cases, mitochondrial function is disrupted.[14] One possible inference from these results is that bisamidines may often have more than one target, with so-called "multi-target" inhibitors being

of interest because they could be less prone to the development of spontaneous resistance due to target mutations, with multi-target inhibition[15] being thought to be one of the main reasons that some antibiotics have been relatively successful in mono-therapy.[16]

The bisamidines **6, 7** and several related compounds have also been shown to bind to bacterial DNA (as observed by fluorescence – the DNA-bound ligands are highly fluorescent) and, more specifically, AT-rich DNA[11,12,17] in which hydrogen-bonding between the ligand and DNA bases can occur.[18] What is interesting here is that, in addition to these bisamidines binding to bacterial DNA, DNA-binding is also the proposed mechanism of action of several of the bisamidines that have been developed as anti-trypanosomatid drug leads (that reached clinical trials) where it is kinetoplast DNA (k-DNA) that is targeted.[17] DNA minor groove binders have also been developed to target a broad range of fungal and bacterial pathogens including *Clostridium difficile*,[19] so the possibility exists that it might be possible to develop compounds that target both DNA as well as a pathogen enzyme target (e.g. UPPS or FPPS), improving selectivity.

In this work, we synthesized a range of amidines and bisamidines and tested them, as well as other known bisamidines, for their binding to (or inhibition of) *E. coli* UPPS, *S. aureus* UPPS, and an AT-rich DNA-duplex $(CGCGAATTCGCG)_2$ and correlated these results with their effects on *S. aureus* and *E. coli* cell growth. In some cases we found both DNA minor groove binding as well as UPPS inhibition, leading to predictive models of cell growth inhibition. We also solved three X-ray structures of some of the leads bound to the DNA dodecamer duplex, in addition to determining three UPPS X-ray structures.

Results and Discussion

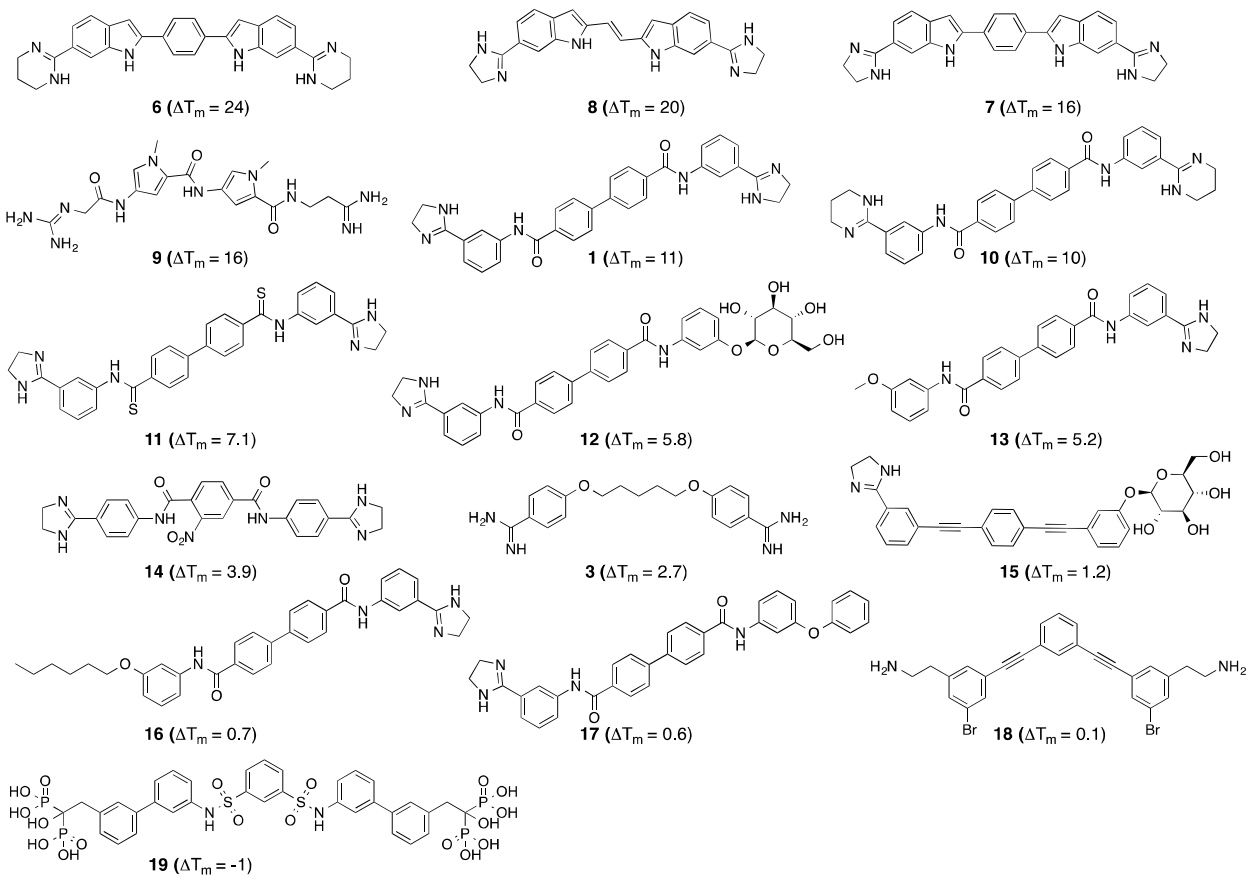

Figure 1. Structures of compounds of interest, discussed in the Text. Compounds are rank ordered (top left to bottom right) by their effects on the folded-unfolded transition (ΔT_m) of a DNA dodecamer duplex $(CGCGAATTCGCG)_2$, as determined by differential scanning calorimetry, the most potent binder being at the top left of the Figure.

We investigated the compounds shown in Figure 1 for their effects on enzyme (*E. coli* UPPS, *S. aureus* UPPS) inhibition, *E. coli* and *S. aureus* cell growth inhibition, and on the folded-unfolded transition of the AT-rich DNA dodecamer duplex, $(CGCGAATTCGCG)_2$. Compounds **6-8** have known anti-bacterial activity and were discovered or developed by Microbiotix (Worcester, MA) from a DTP/NCI (Developmental Therapeutics Program/National Cancer Institute) screening library (**6** = MBX-1162; **7** = MBX-1066 = NSC-317881; **8** = MBX-

1090 = NSC-317880); **9** is the anti-bacterial netropsin; **1** is the bisamidine (NSC 50460) reported previously[5,6] to be a potent UPPS, FPPS inhibitor active against *S. aureus in vitro* and *in vivo*. Compounds **10-13, 16-17** are all analogs of **1** or **10** containing various side-chain or backbone modifications (see Experimental Section for synthesis and characterization); **14** is a Wander A.G. compound (NSC-60340); **3** is pentamidine; **15** is an amidine based on the synthetic antimicrobial **18**[20] (which contains the "cationic-hydrophobic-cationic" motif found in the bisamidines). Compound **19** is a very potent UPPS inhibitor (IC_{50} ~400 nM), but is not expected to bind to DNA (since it is highly anionic).

Enzyme Inhibition. We first tested all 16 compounds against UPPS from *E. coli* and *S. aureus*. Results are shown in Table 1. The compounds are rank-ordered by their ΔT_m values, the strongest DNA-binder being at the top of the Table. As can be seen in Table 1, **1** in the most potent inhibitor of both *E. coli* UPPS (EcUPPS) as well as *S. aureus* UPPS (SaUPPS) with an IC_{50} = 110 nM. The tetraphosphonate **19** is also a potent UPPS inhibitor with an IC_{50} ~400 nM against both enzymes. The bisindole **6** likewise has potent activity against both enzymes and **7** (the same structure as **6** except for the replacement of the 6-membered bisamidine ring by a 5-membered ring) has good activity against EcUPPS (IC_{50} = 360 nM) but less (IC_{50} = 1.7 μM) against SaUPPS. Several other compounds (**13**, **18**) have low or sub-micromolar activity against SaUPPS, but are less active against EcUPPS. Clearly, the overall most active compounds are **1**, **6**, **7** and **19**. Compounds **1**, **6**, **7** are bisamidines while **19** is a tetraphosphonate. With the analogs of **1**, replacement of the 5-membered ring by a 6 membered ring reduced UPPS inhibition activity by 50 fold (Table 1) and replacement of the amide by a thioamide (**1** → **11**) reduced activity by a similar amount. Other side-chain modifications all greatly reduced activity.

Table 1. Enzyme inhibition, cell growth inhibition and differential scanning calorimetry results.

cpd	EcUPPS IC_{50} (μM)	SaUPPS IC_{50} (μM)	*E. coli* EC_{50} (μM)	*S. aureus* EC_{50} (μM)	ΔT_m (°C)
6	0.68	0.47	0.24	0.028	24
8	12	5.1	1.2	0.11	20
7	0.36	1.7	0.33	0.029	16
9	1400	1000	570	11	16
1	0.11	0.11	0.30	0.29	11
10	5.5	4.5	0.66	0.23	10
11	9.2	3.5	58	3.0	7.1
12	380	530	>1500	570	5.8
13	9.4	2.1	570	7.7	5.2
14	4.8	4.9	14	28	3.9
3	400	240	12	4.2	2.7
15	14	5.6	900	380	1.2
16	25	8.9	>1500	280	0.7
17	11	5.7	>1500	10	0.6
18	6.1	1.4	0.97	7.6	0.1
19	0.36	0.39	>1500	100	-1

Cell growth inhibition results. With these results on UPPS inhibition in hand, we next investigated the activity of all 16 compounds against two bacteria, the Gram-negative *E. coli*, and the Gram-positive, *S. aureus*. Cell growth inhibition results are shown in Table 1. As can be seen in Table 1, there are 4 compounds with <1 μM activity against both organisms **1**, **6**, **7**, and **10**, with similar results for **6-8** having been reported previously.[9,11,12,17] In most cases, these four compounds have good activity against UPPS, the exception being **10** (where UPPS IC_{50} values are ~5 μM). However, the potent UPPS inhibitor **19** had no cell activity, presumably because it has poor permeability and in previous work[21] we found only one related (bisphosphonate) inhibitor having activity (EC_{50} = 33 μM), against *E. coli*. These results appear to be in accord with the idea that UPPS could be a target for the most potent cell growth inhibitors (some of which have been shown to inhibit cell wall biosynthesis). There is, however, only a very poor overall correlation between enzyme pIC_{50} (= $-\log_{10} IC_{50}$) and cell growth inhibition pEC_{50} values with R^2 = 0.25, p-value = 0.05 for *E. coli*/EcUPPS, and R^2 = 0.16, p-value = 0.12 for the *S. aureus*/SaUPPS results (Supporting Information Table S1). It thus seemed that there might be another, more important target, DNA, since as noted in the Introduction, in other work it has been shown that bisamidines bind to AT-rich DNA, both in bacteria[11] as well as to kinetoplast DNA, in trypanosomatid parasites such as *T. brucei*.[17]

DNA binding: calorimetry and crystallography. We thus next investigated the binding of the 16 compounds shown in Table 1 to a DNA dodecamer duplex containing an AT-rich central domain: $(CGCGAATTCGCG)_2$, used previously to study the binding of Hoechst 33258,[22] propamidine[23] (pentamidine but with a C_3 linker) and other ammonium compounds.[24] We used differential scanning calorimetry (DSC) to study the DNA-ligand interaction, and DSC

thermograms for all 16 compounds are shown in Figure 2 (the results for the compounds having the largest ΔT_m values being shown at top left).

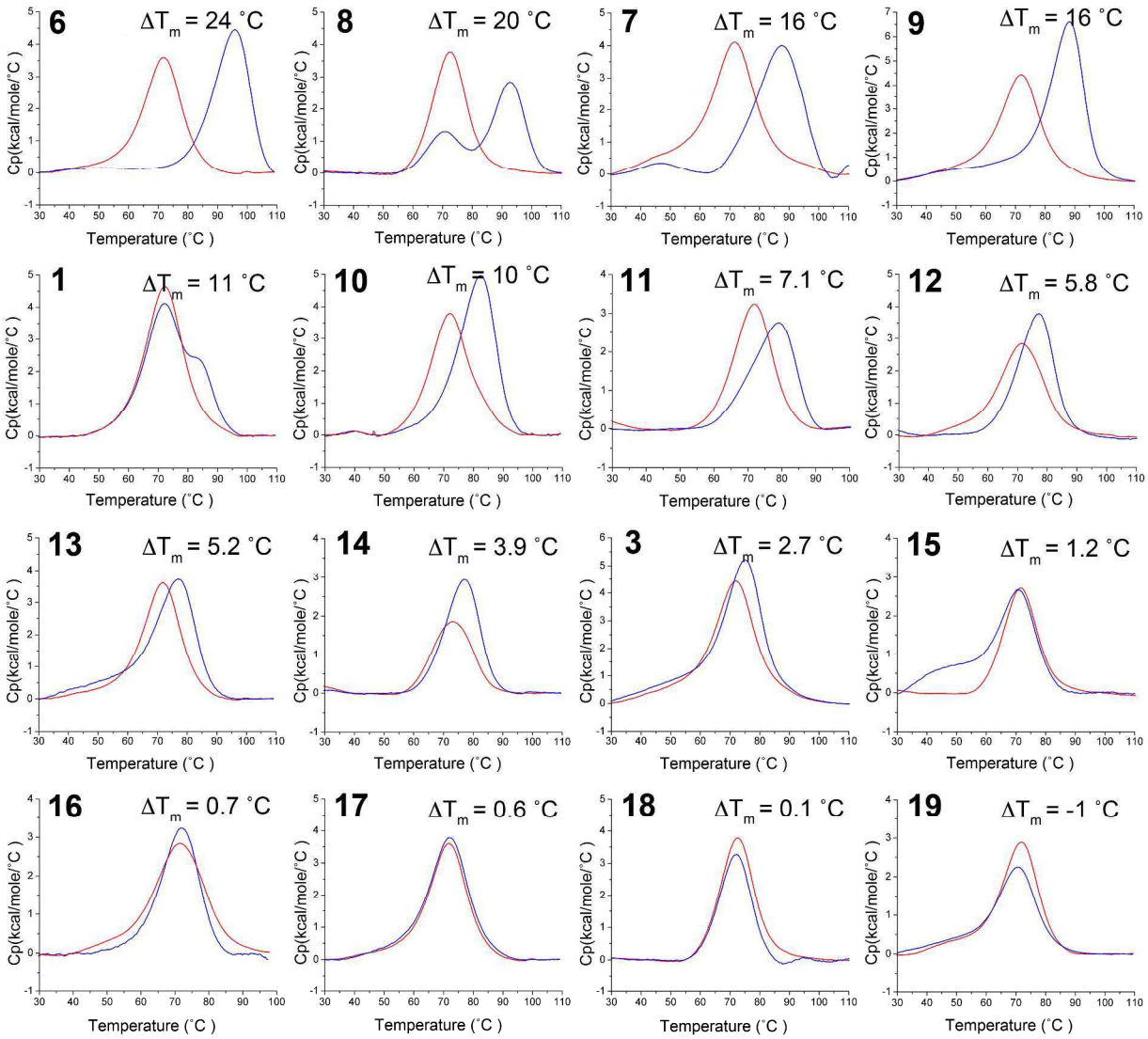

Figure 2. DSC thermograms for the 16 compounds shown in Figure 1 binding to the DNA dodecamer duplex $(CGCGAATTCGCG)_2$. The ΔT_m values are indicated. Apo-DNA thermograms of are shown in red and DNA/ligand (1:1) thermograms are shown in blue.

The changes in the DNA thermal unfolding temperatures, ΔT_m (where T_m is the maximum in the C_p vs. T thermogram) are given in Table 1 and the DSC thermogram results are shown in Figure 2, ranked according to their ΔT_m values. In most cases there was a single component observed, although in several instances there were two components (folded + unfolded), due presumably to solubility/incomplete mixing deficiencies. The two strongest binding ligands were **6** (ΔT_m = 24 ˚C) and **8** (ΔT_m = 20 ˚C), followed by **7** (ΔT_m = 16 ˚C) and **9** (netropsin, ΔT_m = 16˚C). **1**, the 5 membered biphenyl bisamidine had ΔT_m = 11 ˚C, essentially the same as the 6-membered ring analog **10** (ΔT_m = 10 ˚C). The thioamide analog of **1**, **11**, had worse binding (ΔT_m = 7.1 ˚C). Pentamidine (**3**) was also a poor binder (ΔT_m = 2.7 ˚C). Clearly, for most potent binding, the presence of a bisamidine is required, together with, perhaps, central groups that might H-bond to the DNA bases. What is particularly interesting about these DSC results is that the most potent DNA binders are also some of the most the potent UPPS inhibitors, as well as the most potent cell growth inhibitors, suggesting, perhaps, dual target inhibition.

To see how some of the bisamidines actually bound to the $d(CGCGAATTCGCG)_2$ duplex, we used X-ray crystallography, co-crystallizing the DNA-ligand complexes as described in the Experimental Section. Full crystallographic data acquisition and structure refinement details are given in Table 2. Ligand electron density maps and ligand-protein interactions are given in Supporting Information Figures S1-4.

As can be seen in Figure 3, **1**, **6** and **10** all bound to the minor groove of the AT-rich dodecamer, and in each case there are H-bond contacts between the nitrogen atoms in the ligands, either in the amidine ring, amide bond (**1** and **10**) or in the indole group (**6**), with the bases in the DNA minor groove. Although there are only 3 structures, more interactions correlate with stronger binding, that is, a bigger ΔT_m: **6** has 6 H-bond contacts and a ΔT_m = 24 ˚C; **1** and

10 have only 3-4 interactions and a $\Delta T_m \sim 10$ ˚C, Figure 3 and Supporting Information Figures S2-4.

Table 2. Data collection and refinement statistics for DNA duplex $(CGCGAATTCGCG)_2$.

	DNA/**1**	DNA/**6**	DNA/**10**
Crystals	(4U8B)	(4U8C)	(4U8A)
Data collection			
Space group	$P2_12_12_1$	$P2_12_12_1$	$P2_12_12_1$
a, *b*, *c* (Å)	23.77, 39.39, 65.36	24.79, 39.95, 65.79	25.18, 40.14, 65.63
Resolution (Å)	50.0-1.31 (1.33-1.31)	50.0-1.24 (1.26-1.24)	50.0-1.48 (1.52-1.48)
No. of reflections	15,205 (731)	18,244 (760)	11,466 (533)
Completeness (%)	98.7 (100.0)	95.0 (83.2)	98.3 (97.1)
R-merge	0.076 (0.66)	0.068 (0.55)	0.050 (0.39)
I/σ(I)	29.8 (5.4)	32.8 (3.6)	44.5 (5.9)
Multiplicity	13.4 (14.3)	13.8 (12.1)	13.8 (12.9)
Refinement statistics			
R-work/*R*-free (%)	24.2/24.6	27.6/33.3	26.6/32.2
Geometry deviations			
Bond lengths (Å)	0.019	0.015	0.015
Bond angles (°)	2.76	2.33	2.84
B average ($Å^2$)/No. of non-H atoms			
DNA	19.7/486	22.8/486	26.1/486
Water	20.2/43	30.5/17	21.6/30
Ligand	39.5/40	26.3/36	22.9/42

Values in parentheses correspond to the highest-resolution shells.

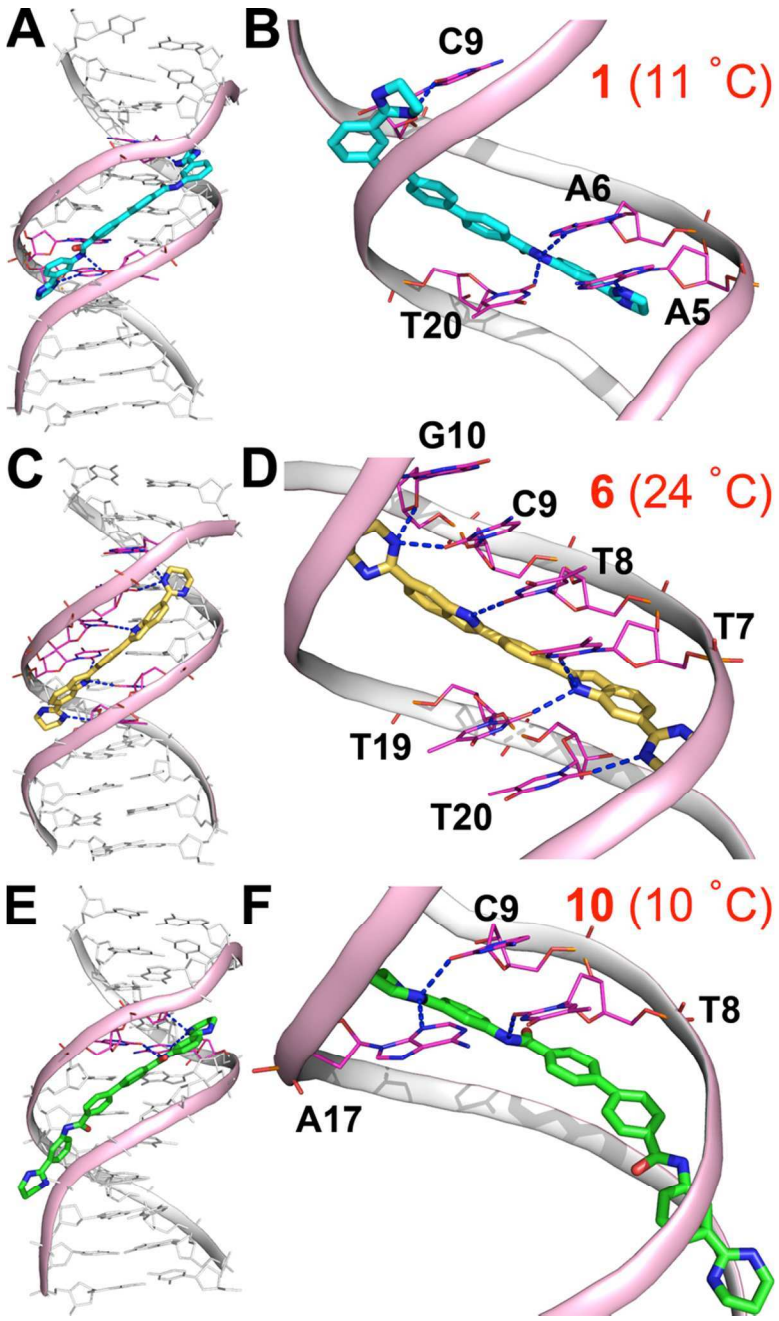

Figure 3. X-ray structures of DNA dodecamer duplex $(CGCGAATTCGCG)_2$ showing bisamidines bind to minor groove and interact with the nucleobases. (A) **1** (cyan) binds to the DNA minor groove and (B) interacts with A5, A6, C9 and T20 (pink). (C) **6** (yellow) binds to the DNA minor groove and (D) interacts with T7, T8, C9, G10, T19, and T20 (pink). (E) **10** (green) binds to the DNA minor groove and (F) interacts with T8, C9, and A17 (pink). The

largest number of bisamidine contacts correlates with the largest ΔT_m value (shown in parentheses).

Models for cell growth inhibition. These DSC ΔT_m results now enable us to test the hypothesis that the cell-based activity we see could be due to DNA binding, to UPPS binding, or to both DNA as well as UPPS binding. We first used a simple heat-map approach, Figure 4A, from which it can be seen that *S. aureus* cell growth inhibition can be quite potent and is most strongly correlated with ΔT_m (both in red/orange), with a weaker correlation with SaUPPS inhibition (Figure 4A). The trends are similar with *E. coli* (Figure 4A). The quantitative correlation between cell growth inhibition and either pIC_{50} (UPPS) or DNA ΔT_m results are however poor, as shown in Table S1, varying from 0.16 to 0.60. We thus next employed the basic approach derived earlier[25] in which we used Eqn. 1:

$$pEC_{50}\ (\text{cell}) = a \bullet A + b \bullet B + c \bullet C + d \qquad \text{(Eqn. 1)}$$

where in this case A = UPPS pIC_{50}, B = DNA ΔT_m and C is an (optional) computed descriptor (selected from 307 descriptors we computed in MOE[26]). With the UPPS pIC_{50} and DNA ΔT_m data together, the correlations improved to $R^2 = 0.73$, $p = 0.0002$ for *S. aureus* and $R^2 = 0.53$, $p = 0.008$ for *E. coli*, Table S1. These results improved further with addition of a computed descriptor (vsurf_ID5 for *S. aureus*; GCUT_SMR_3 for *E. coli*) to $R^2 = 0.89$, $p = 4\times10^{-6}$ for *S. aureus* and $R^2 = 0.78$, $p = 0.0003$ for *E. coli* (Table S1). The ΔT_m term was the major contributor to the *S. aureus* model while both UPPS inhibition and DNA binding contributed to the *E. coli* model. The experimental versus computed cell pEC_{50} results are shown in Figures 4B, C. There was no significant correlation between pIC_{50} (EcUPPS) and ΔT_m ($R^2 = 0.02$, $p = 0.6$), or between pIC_{50} (SaUPPS) and ΔT_m ($R^2 = 0.003$, $p = 0.8$) when data for all 16 compounds was used.

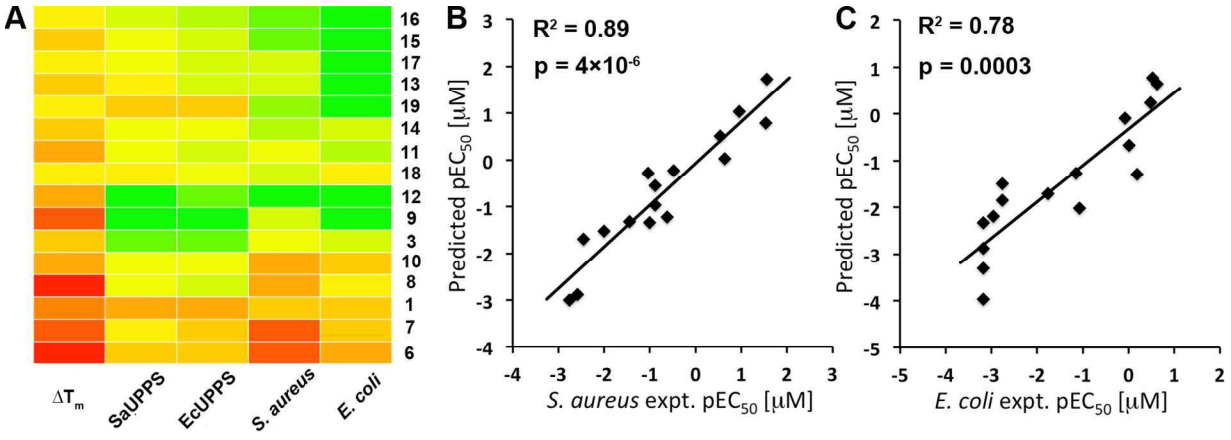

Figure 4. Heat-map and correlation plot. (A) Enzyme and cell growth inhibition and DNA binding heat-map. Red = strong activity; yellow = moderate activity; green = weak/no activity. (B) Correlation plot for *S. aureus* experimental and predicted cell activities based on UPPS IC_{50} and DNA ΔT_m results in addition to 1 mathematical descriptor (vsurf_ID5). (C) Correlation plot for *E. coli* experimental and predicted cell activities based on UPPS IC_{50} and DNA ΔT_m results in addition to 1 mathematical descriptor (GCUT_SMR_3).

These results suggest, then, an extended model for the potent *S. aureus* growth inhibition reported previously[6] for **1** in which there is multi-target inhibition (DNA binding as well as UPPS inhibition), consistent with the observed synergistic interaction seen with meticillin in a meticillin-resistant strain of *S. aureus*, as illustrated schematically in Figure 5.

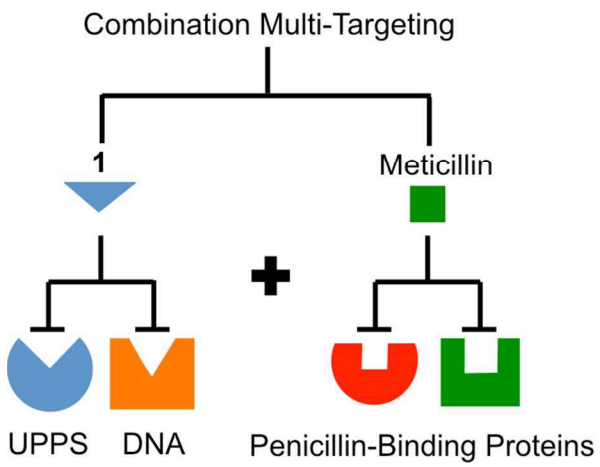

Figure 5. Schematic illustration of combination multi-targeting in *S. aureus*. **1** inhibits UPPS as well as binding to AT-rich bacterial DNA and synergizes with meticillin (FICI = 0.25) since UPPS inhibition decreases flux though the isoprenoid biosynthesis pathway, required for peptidoglycan formation (via undecaprenyl phosphate, Lipid I and Lipid II).

X-ray structures of SaUPPS and EcUPPS: progress and puzzles. Finally, we sought to investigate how some of the UPPS inhibitors bound to UPPS. The SaUPPS protein was of most interest since inhibitors such as **1** bind tightly to SaUPPS and are active *in vivo*. At present, there have been no reports of the structures of SaUPPS with (or without) inhibitors, although there are two reported structures of SaUPPS with its FPP substrate.[6,27] Unfortunately, we were not successful in obtaining any bisamidine-bound SaUPPS X-ray structures, but we did obtain the structure of apo-UPPS as well as that of a S-*thiolo* farnesyl diphosphate (FSPP) inhibitor (IC_{50} = 1.9 μM). Full crystallographic data acquisition and structure refinement details (PDB ID codes 3WYI, 4U82) are given in Table 3. Ligand electron density maps and ligand-protein interactions are given in Supporting Information Figures S5 and S6. The *apo*-SaUPPS structure (Figure 6A) has a 1.4 Å Cα residue mean square deviation (rmsd) from the EcUPPS *apo* structure (PDB ID code 3QAS), while the FSPP-SaUPPS structure (Figure 6B) has a 1.1 Å rmsd

from the FSPP-EcUPPS structure (PDB ID code 1X06). These two proteins have a 43% sequence identity and 62% similarity as calculated by BLAST analysis.[28] These strong sequence and structural similarities suggest that SaUPPS bisamidine inhibitors should bind in a similar manner to that seen with EcUPPS, to i.e. sites 2, 4 as reported previously.[6] The question then arises as to why we were unsuccessful in obtaining SaUPPS bisamidine-bound structures. One likely possibility is that since in the *apo*-SaUPPS structure, residues 77-84 (shown in red in Figure 6A, B) form a loop that blocks entrance to the binding pocket, at least in the crystal. In the FSPP-inhibitor structure, the loop is displaced, as shown in Figure 6C, D, and FSPP, Mg^{2+} and sulfate are clearly visible. The molecular basis for this pocket closure in the *apo* form is not obvious, but may simply be due to lattice packing effects (since both SaUPPS and EcUPPS are inhibited by bisamidines, in solution). The inability to obtain a bisamidine-bound SaUPPS structure was also reflected in our inability to obtain a structure with another large inhibitor **19**, consistent with a lattice-packing effect (since **19** is also a good SaUPPS inhibitor, in solution). We did succeed, however, in obtaining a structure of **19** bound to EcUPPS, Figure 7.

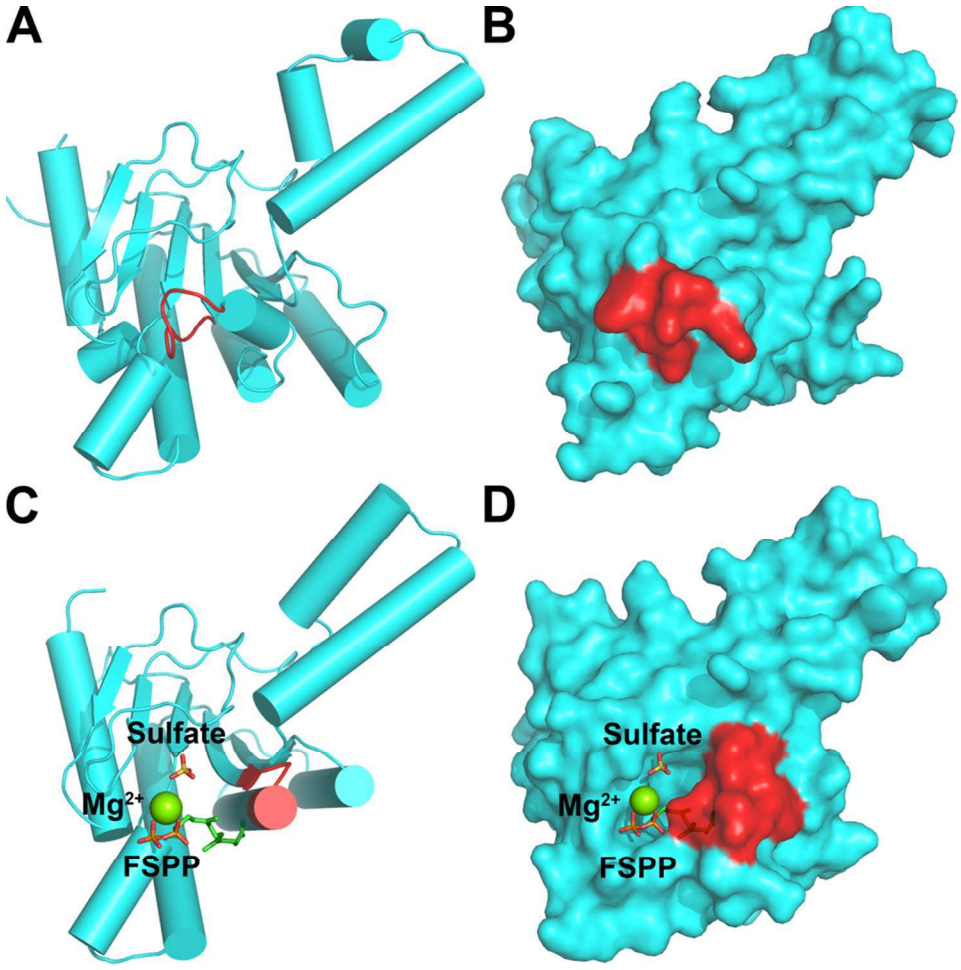

Figure 6. X-ray structures of *S. aureus* UPPS. (A) Closed structure found in *apo*-SaUPPS, 77-84 in red (PDB ID code 3WYI). (B) Protein surface representation of apo structure. (C) Ligand bound UPPS showing FSPP, sulfate and Mg^{2+}, open pocket, residues 77-84 in red (PDB ID code 4U82). (D) Protein surface representation of FSPP-bound structure.

As reported previously,[29] small bisphosphonates bind to EcUPPS with their lipophilic side-chains binding to one or more of sites 1, 2, 3 or 4,[29] as shown for the inhibitor BPH-629 ([2-(3-(dibenzofuran-2-yl-phenyl)-1-hydroxy-1-phosphono-ethyl]-phosphonic acid) in Figure 7A. However, with the bisamidine **14** (Figure 7B) as well as the diacetylenic amine species **18** (which would be expected to protonated), only a single molecule bound to UPPS, and these molecules were found to span both sites 2 and 4, the cationic groups being relatively solvent

exposed, while the aromatic groups were buried in the hydrophobic interior of the protein. With **19**, we found that sites 1-3 were all occupied, Figure 7C. Full crystallographic data acquisition and structure refinement details (PDB ID code 3WYJ) are given in Table 3. Ligand electron density maps and ligand-protein interactions are given in Supporting Information Figure S7-8.

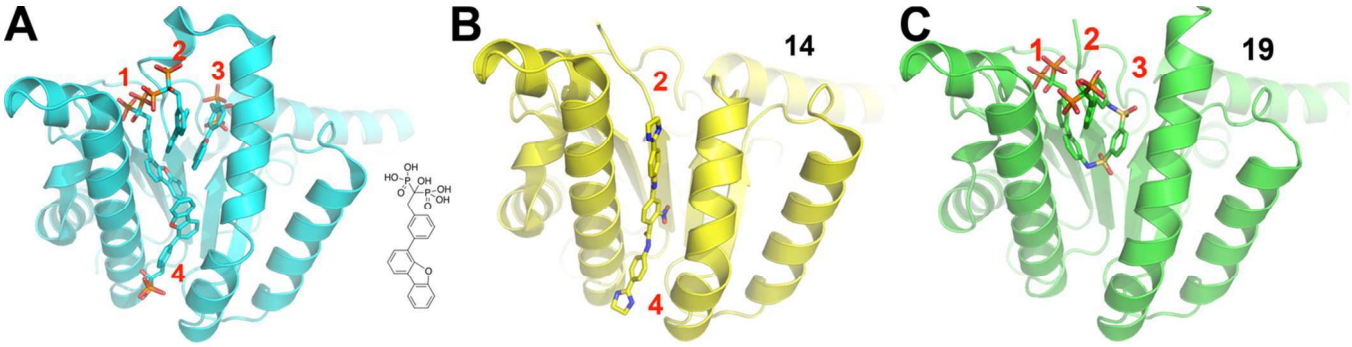

Figure 7. X-ray structures of *E. coli* UPPS showing ligand binding sites. (A) The bisphosphonate shown binds to sites 1-4 (PDB ID code 2E98). (B) Bisamidine **14** binds to sites 2 and 4 (PDB ID code 4H2J). (C) The tetraphosphonate **19** binds to sites 1-3 (PDB ID code 3WYJ).

Table 3. Data collection and refinement statistics for UPPS.

	SaUPPS/*Apo*	SaUPPS/FSPP	EcUPPS/**19**
Crystals	(3WYI)	(4U82)	(3WYJ)
Data collection			
Space group	$P3_121$	$P4_12_12$	$P2_12_12_1$
a, *b*, *c* (Å)	62.08, 62.08, 133.49	57.08, 57.08, 158.62	63.71, 69.00, 108.89
Resolution (Å)	25.0-2.0 (2.07-2.00)	50.0-1.66 (1.69-1.66)	25.0-2.1 (2.18-2.10)
No. of reflections	20,923 (2,047)	32,040 (1,573)	28,793 (2,803)
Completeness (%)	100.0 (100.0)	100.0 (99.8)	99.7 (99.7)
R-merge	0.066 (0.50)	0.068 (0.70)	0.049 (0.36)
I/σ(I)	32.8 (3.6)	34.6 (4.6)	39.1 (6.0)
Multiplicity	8.5 (8.2)	14.3 (14.3)	5.8 (5.4)
Refinement statistics			
R-work/*R*-free (%)	19.0/22.7	18.7/22.0	20.0/24.1
Geometry deviations			
Bond lengths (Å)	0.015	0.026	0.006
Bond angles (°)	1.20	2.42	1.15
B average (Å^2)/No. of non-H atoms			
Protein	36.1/1894	19.4/1930	36.6/3504
Water	55.4/382	23.7/84	53.6/426
Ligand	-	25.3/25	57.4/60
Ramachandran plot			
Most favored (%)	96.5	97.9	97.2
Allowed (%)	3.5	2.1	2.5
Disallowed (%)	0	0	0.2

Values in parentheses correspond to the highest-resolution shells.

Conclusions

The results we have reported here are of interest for a number of reasons. First, we synthesized and tested a range of amidine and bisamidine compounds against *E. coli* and *S. aureus* UPPS finding quite potent activity with some bisamidines. Second, we found that several bisamidines also bound to AT-rich DNA, shifting T_m by as much as 24 ˚C. Third, we developed computational models for cell growth inhibition using DNA ΔT_m and UPPS pIC_{50} values together with one mathematical descriptor that had R^2 = 0.78-0.90. Fourth, we determined the structures of 3 bisamidines bound to a synthetic DNA $(CGCGAATTCGCG)_2$ finding minor groove binding, with the largest ΔT_m correlating with the largest number of ligand-DNA interactions. Fifth, we solved three UPPS structures. Overall, the most important finding is that the compounds with best cell growth inhibition bind to AT-rich DNA in addition to inhibiting UPPS. This is a potentially important observation since it could lead to novel therapeutic leads that inhibit bacterial cell wall biosynthesis (targeting UPPS), synergize with existing drugs acting in these pathways (as does **1** with meticillin in a meticillin-resistant *S. aureus* strain), and also inhibit DNA replication: multiple-targeting leads that could in some cases help reverse resistance. It is, however, also possible that there may be toxicity against a potential host with such multi-target inhibitors although EC_{50} values against mammalian cells (manuscript in preparation) for compound **1** are >100 μM, leading to selectivity indices with *S. aureus* of > 300. Moreover, **1** showed no adverse side-effects in the *S. aureus* mouse model of infection[6] and **7** and **8** have been reported to be effective in mice models of infection with both *Bacillus anthracis* as well as *Yersinia pestis*.[11]

Experimental section

Chemical Syntheses: General Methods. All chemicals were reagent grade. Pentamidine and netropsin were purchased from Aldrich. ^{1}H NMR and ^{13}C NMR spectra were obtained on Varian (Palo Alto, CA) Unity spectrometers at 400 and 500 MHz for ^{1}H and at 100 and 125 MHz for ^{13}C. Elemental analyses were carried out in the University of Illinois Microanalysis Laboratory. HPLC/MS analyses were performed by using an Agilent LC/MSD Trap XCT Plus system (Agilent Technologies, Santa Clara, CA) with an 1100 series HPLC system including a degasser, an autosampler, a binary pump, and a multiple wavelength detector. All final compounds were ≥95% pure as determined by elemental analysis or analytical HPLC/MS analysis and were also characterized by ^{1}H NMR and HRMS.

N4,N4'-bis(3-(4,5-dihydro-1H-imidazol-2-yl)phenyl)-[1,1'-biphenyl]-4,4'-bicarboxamide (1)

To a mixture of 4,4'-diphenyl dicarbonyl chloride (1.39 g, 5 mmol), 3-aminobenzonitrile (1.18 g, 10 mmol) in anhydrous THF (20 mL) was added Et_3N (2.1 mL, 15 mmol) and the mixture stirred at room temperature overnight. After filtration, the white solid was washed with water (20 mL) and ethyl acetate (10 mL) and then dried. Sodium hydrosulfide hydrate (100 mg), ethylenediamine (2 mL), and dimethylacetamide (10 mL) were then added and stirred overnight at 140 °C. Upon solvent removal, the solid was washed thoroughly with water and then ethyl acetate (10 mL). To a suspension of the crude product in 10 mL of water were added two equivalents of methanesulfonic acid. Removal of water afforded the final product **1** as its methanesulfonic acid salt (1.44 g, 40%). ^{1}H NMR (DMSO-d_6, 500 MHz) δ: 10.68 (s, 2 H), 10.52 (s, 4 H), 8.50 (s, 2 H), 8.12 (d, J = 9.0 Hz, 4 H), 8.02–7.98 (m, 2 H), 7.96 (d, J = 9 Hz, 4 H), 7.68–7.58 (m, 4 H), 4.00 (s, 8 H), 2.36 (s, 6 H). HRMS (ESI): m/z $[M + H]^+$ calculated for

$C_{32}H_{29}N_6O_2$ 529.2361, found 529.2352. Purity of the product determined by HPLC (Phenomenex C6-Phenyl 110A. 100×2 mm, 3 μm, 300 nm, retention time = 5.6 min): 98.9%.

1,4-bis(6-(1,4,5,6-tetrahydropyrimidin-2-yl)-1*H*-indol-2-yl)benzene (6)

Terephthalaldehyde (1.34 g, 10 mmol) and 4-methyl-3-nitrobenzonitrile (3.24 g, 20 mmol) were added to a round-bottom flask and heated to 150 ^{o}C until the compounds melted. Piperidine (1.5 mL) and sulfolane (10 mL) were added and the resulting solution stirred at 150 ^{o}C overnight then cooled to room temperature to yield an orange solid (3.4 g, 80%) which was washed with methanol (15 mL ×3) and dried. The solid, 4,4'-(1*E*,1'*E*)-2,2'-(1,4-phenylene)bis(ethene-2,1-diyl)bis(3-nitrobenzonitrile) was then suspended in triethyl phosphate (30 mL) and heated to reflux (160 ^{o}C) for 72 h until the mixture turned from orange to yellow. The suspension was filtered and the yellow solid washed with methanol (15 mL ×3) and dried (1.4 g, 55%). The solid 2,2'-(1,4-phenylene)bis(1*H*-indole-6-carbonitrile) was suspended in propane-1,3-diamine (15 mL) and heated to 130 ^{o}C for 24 h. The suspension was filtered and the solid washed with water (15 mL ×3) and methanol (15 mL ×3). The final product **6** was a yellow solid. ^{1}H NMR (DMSO-d_6, 500 MHz) δ: 7.99 (s, 4 H), 7.79 (s, 2 H), 7.48 (d, J = 8.0 Hz, 2 H), 7.42 (d, J = 8.0 Hz, 2 H), 6.99 (s, 2 H), 3.37 (s, 8 H), 1.72 (m, 4 H). HRMS (ESI): m/z $[M + H]^+$ calculated for $C_{30}H_{29}N_6$ 473.2454, found 473.2450. Purity of the product determined by HPLC (Phenomenex C6-Phenyl 110A. 100x2 mm, 3 μm, 230 nm, retention time = 5.8 min): 99.1%.

1,4-bis(6-(4,5-dihydro-1*H*-imidazol-2-yl)-1*H*-indol-2-yl)benzene (7)

Terephthalaldehyde (1.34 g, 10 mmol) and 4-methyl-3-nitrobenzonitrile (3.24 g, 20 mmol) were added to a round-bottom flask and heated to 150 ^{o}C until the compounds melted. Piperidine (1.5 mL) and sulfolane (10 mL) were added and the resulting solution stirred at 150 ^{o}C overnight then cooled to room temperature to yield an orange solid (3.4 g, 80%) which was

washed with methanol (15 mL ×3) and dried. The solid 4,4'-(1*E*,1'*E*)-2,2'-(1,4-phenylene)bis(ethene-2,1-diyl)bis(3-nitrobenzonitrile) was then suspended in triethyl phosphate (30 mL) and heated to reflux (160 ^{o}C) for 72 h until the mixture turned from orange to yellow. The suspension was then filtered and the yellow solid washed with methanol (15 mL ×3) and dried (1.4 g, 55%). The solid 2,2'-(1,4-phenylene)bis(1*H*-indole-6-carbonitrile) was suspended in ethane-1,2-diamine (15 mL) and heated to 130 ^{o}C for 24 h. The suspension was filtered and the solid washed with water (15 mL ×3) and methanol (15 mL ×3). The final product **7** was a yellow solid. ^{1}H NMR (DMSO-d_6, 500 MHz) δ: 11.73 (s, 2 H), 7.97 (s, 4 H), 7.85 (s, 2 H), 7.50 (s, 4 H), 7.00 (s, 2 H), 3.28 (s, 4 H). HRMS (ESI): m/z $[M + H]^+$ calculated for $C_{28}H_{25}N_6$ 445.2141, found 445.2139. Purity of the product determined by HPLC (Phenomenex C6-Phenyl 110A. 100×2 mm, 3 μm, 230 nm, retention time = 5.5 min): 99.3%.

1*H*-Indole, 2,2'-(1,2-ethenediyl)bis[6-(4,5-dihydro-1*H*-imidazol-2-yl) dihydrochloride (8)

The compound was obtained from the Drug Synthesis and Chemistry Branch, Developmental Therapeutics Program, Division of Cancer Treatment and Diagnosis, National Cancer Institute. ^{1}H NMR (methanol-d_4, 400 MHz): 7.92 (s, 2H), 7.71 (d, 8.4 Hz, 2H), 7.45 (d, J = 8.8 Hz, 2H), 7.33 (s, 2H), 6.78 (s, 2H), 4.08 (s, 4H). HRMS (ESI): m/z $[M + H]^+$ calculated for $C_{24}H_{23}N_6$ 395.1984, found 395.1986. Purity of the product determined by HPLC (Phenomenex C6-Phenyl 110A. 100×2 mm, 3 μm, 230 nm, retention time = 5.6 min): 97.2%.

N4,N4'-bis(3-(1,4,5,6-tetrahydropyrimidin-2-yl)phenyl)biphenyl-4,4'-dicarboxamide (10)

To a mixture of 4,4'-diphenyl dicarbonyl chloride (1.39 g, 5 mmol), 3-aminobenzonitrile (1.18 g, 10 mmol) in anhydrous THF (20 mL) was added Et_3N (2.1 mL, 15 mmol) and the mixture stirred at room temperature, overnight. After filtration, the white solid was washed with water (20 mL) and ethyl acetate (10 mL) and then dried. Sodium hydrosulfide hydrate (100 mg),

propane-1,3-diamine (2 mL), and dimethylacetamide (10 mL) were then added and the mixture stirred overnight at 140 °C. Upon solvent removal, the solid was washed with water and then ethyl acetate (10 mL). To the suspension of the crude product in 10 mL of water were added two equivalents of methanesulfonic acid. Removal of water afforded the final product as its methanesulfonic acid salt (1.50 g, 40%). ^{1}H NMR (DMSO-d_6, 500 MHz) δ: 10.68 (s, 2 H), 9.95 (s, 4 H), 8.38 (s, 2 H), 8.14 (d, J = 9.0 Hz, 4 H), 7.98 (m, 6 H), 7.62 (t, 2 H), 7.42 (d, 2 H), 3.50 (s, 8 H), 2.29 (s, 4 H). HRMS (ESI): m/z $[M + H]^+$ calculated for $C_{34}H_{33}N_6O_2$ 557.2665, found 557.2658. Purity of the product determined by HPLC (Phenomenex C6-Phenyl 110A. 100×2 mm, 3 μm, 230 nm, retention time = 5.3 min): 99.6%.

N4,N4'-bis(3-(4,5-dihydro-1*H*-imidazol-2-yl)phenyl)biphenyl-4,4'-bis(carbothioamide) (11)

N4,N4'-bis(3-(4,5-dihydro-1*H*-imidazol-2-yl)phenyl)-[1,1'-biphenyl]-4,4'-bicarboxamide (**1**, 560 mg, 1 mmol) was suspended in pyridine (5 mL). Lawesson's reagent (2,4-bis(4-methoxyphenyl)-1,3,2,4-dithiadiphosphetane-2,4-disulfide) (1.0 g, 2.5 mmol) was added and the mixture heated to 150 ^{o}C for 72 h at which point the mixture had turned yellow. The suspension was then filtered and the solid washed with methanol (15 mL ×3) and acetone (15 mL ×3) and then dried under vacuum. The product **11** was obtained as a yellow solid. ^{1}H NMR (DMSO-d_6, 500 MHz) δ: 12.12 (s, 2 H), 10.60 (s, 4 H) 8.45 (s, 2 H), 7.90 (d, J = 9.0 Hz, 4 H), 8.00–7.98 (m, 2 H), 7.82 (d, J = 9 Hz, 4 H), 7.73 (m, 4 H), 4.00 (s, 8 H). HRMS (ESI): m/z $[M + H]^+$ calculated for $C_{32}H_{29}N_6S_2$ 561.1895, found 561.1896. Purity of the product determined by HPLC (Phenomenex C6-Phenyl 110A. 100×2 mm, 3 μm, 230 nm, retention time = 5.8 min): 97.6%.

N^4-(3-(4,5-dihydro-1*H*-imidazol-2-yl)phenyl)-$N^{4'}$-(3-(((2S,3R,4S,5S,6R)-3,4,5-trihydroxy-6-(hydroxymethyl)tetrahydro-2*H*-pyran-2-yl)oxy)phenyl)-[1,1 -biphenyl]-4,4 –dicarboxamide (12)

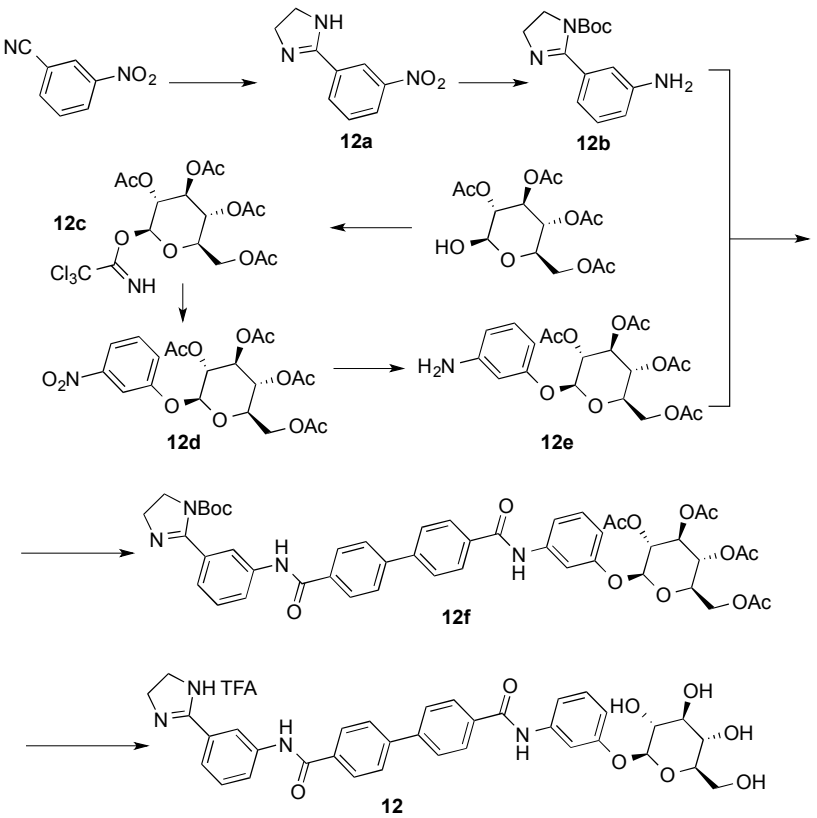

3-nitrobenzonitrile (3.6 g, 20 mmol) was treated with ethylene diamine (40 mL) and NaHS (200 mg). The solution was heated at 110 ^{o}C for 48 h and then quenched with water. The residue was extracted with ethyl acetate, dried under vacuum and purified by flash chromatography (silica gel, hexane/ethyl acetate = 2/1) to give the dihydroimidazole compound **12a** (2.6 g, 60%). To a solution of **12a** (2.2 g, 10 mmol) and $NaHCO_3$ (3.6 mg, 40 mmol) in dichloromethane (20 mL) and water (20 mL) was added $(Boc)_2O$ (4.5 g, 20 mmol) with vigorous stirring at 0 ^{o}C. Stirring was continued for 12 h at which point the mixture had to room temperature. The dichloromethane phase was separated and concentrated to give the Boc protected nitro compound. To the Boc protected nitro compound in ethyl acetate (40 mL) was added Pd/C (10% palladium on charcoal, 145 mg) under nitrogen at room temperature. The nitrogen was switched to H_2 using a balloon and stirring was continued for 12 h at room temperature. Filtration and concentration under reduced pressure gave the 3-aminophenyl

imidazoline **12b**. Glucose tetraacetate (3.5 g, 10 mmol) was treated with trichloroacetonitrile (14.4 g, 100 mmol), DBU (0.3 g, 2 mmol) and CH_2Cl_2 (40 mL). The solution was stirred at room temperature for 12 h and then washed with water. The residue was extracted with Et_2O, dried under vacuum and purified by flash chromatography (silica gel, hexane/ethyl acetate = 2/1) to give the peracetyl glucopyranosyl trichloroacetimidate **12c** (4.4 g, 90%). A mixture of **12c** (4.0 g, 8 mmol), 3-nitrophenol (1.1 g, 8 mmol), and freshly activated 4 Å molecular sieves in anhydrous CH_2Cl_2 (30 mL) was stirred under N_2 at 0 ^oC for 10 min, then BF_3•Et_2O (40 μL, 0.8 mmol) was added via syringe. Stirring continued for 3 h, then Et_3N (2 mL) was added, and the resulting mixture filtered through Celite. The filtrate was concentrated and purified by silica gel column chromatography (hexane/ethyl acetate = 3/1) to give 3-nitrophenol glycoside **12d** (3.0 g, 80%). To a solution of **12d** (2.3 g, 5 mmol) in ethyl acetate (20 mL) was added Pd/C (10% palladium on charcoal, 100 mg) under nitrogen at room temperature. The nitrogen was switched to H_2 using a balloon and stirring was continued for 12 h at room temperature. Filtration and concentration under reduced pressure gave 3-aminophenol glycoside **12e**. To a solution of **12b** (520 mg, 2 mmol), **12e** (920 mg, 2 mmol) and Et_3N (1 mL) in dry dichloromethane (20 mL) was added [1,1'-biphenyl]-4,4'-dicarbonyl dichloride (560 mg, 2 mmol) at 0 ^oC. Stirring was continued for 4 h at 0 ^oC. The reaction mixture was washed with water (15 mL ×3), then concentrated under reduced pressure to give the residue. Purification of the residue by chromatography (silica gel, hexane/ethyl acetate = 2/1) gave product **12f** (800 mg, 45%). To a solution of **12f** (450 mg, 0.5 mmol) in MeOH (5 mL) was added MeONa (1 g) at room temperature. Stirring was continued for 4 h at room temperature and all the volatile components were removed under reduced pressure. The resulting residue was purified by chromatography (silica gel, ethyl acetate) to give the non-protected glycoside. To a solution of the free glycoside (360 mg, 0.5 mmol) in

dichloromethane (3 mL) was added trifluoroacetic acid (2 mL) with stirring at room temperature. Stirring was continued for 4 h then all volatile components were removed under reduced pressure. The resulting residue was purified by chromatography (silica gel, chloroform/MeOH = 5/1) to give the final product **12** (340 mg, 95%). ^{1}H NMR (methanol-d_4, 400 MHz) 8.48 (m, 1H), 8.06 (m, 4H), 7.96 (m, 5H), 7.61 (m, 2H), 7.55 (m, 1H), 7.37 (d, J = 8.0 Hz, 1H), 7.26 (t J = 8.0 Hz, 1H), 6.89 (dd, J = 1.6 Hz, 1H), 4.78 (s, 1H), 4.11 (s, 4H), 3.90 (dd, J = 12.0, 2.0 Hz, 1H), 3.71 (dd, J = 12.0, 7.6 Hz, 1H), 3.46-3.38 (m, 5H). HRMS (ESI): m/z $[M + H]^+$ calculated for $C_{35}H_{35}N_4O_8$, 639.2455; found 639.2446. Purity of the product determined by HPLC (Phenomenex C6-Phenyl 110A. 100×2 mm, 3 μm, 210 nm, retention time = 5.8 min): 97.9%.

N^4-(3-(4,5-dihydro-1*H*-imidazol-2-yl)phenyl)-$N^{4'}$-(3-methoxyphenyl)-[1,1-biphenyl]-4,4–dicarboxamide (13)

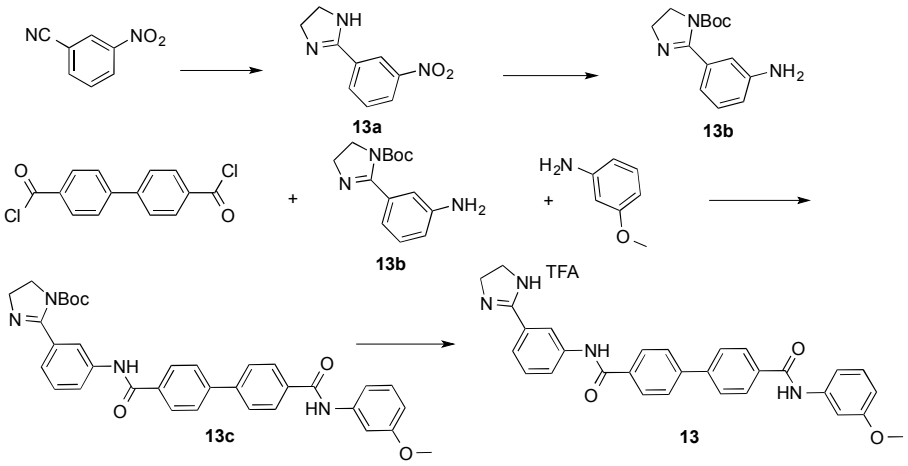

3-nitrobenzonitrile (3.6 g, 20 mmol) was treated with ethylene diamine (40 mL) and NaHS (200 mg). The solution was heated at 110 ^{o}C for 48 h and then quenched with water. The residue was extracted with ethyl acetate, dried under vacuum and purified by flash chromatography (silica gel, hexane/ethyl acetate = 2/1) to give the dihydroimidazole compound **13a** (2.6 g, 60%). To a solution of **13a** (2.2 g, 10 mmol) and $NaHCO_3$ (3.6 mg, 40 mmol) in dichloromethane (20 mL) and water (20 mL) was added $(Boc)_2O$ (4.5 g, 20 mmol) with vigorous

stirring at 0 ^{o}C. Stirring was continued for 12 h at which point the mixture had risen to room temperature. The dichloromethane phase was separated and concentrated to give the Boc protected nitro compound. To a solution of the Boc protected nitro compound in ethyl acetate (40 mL) was added Pd/C (10% palladium on charcoal, 145 mg) under nitrogen at room temperature. The nitrogen was switched to H_2 using a balloon and stirring continued for 12 h at room temperature. Filtration and concentration under reduced pressure gave the crude 3-aminophenyl imidazoline **13b**. To a solution of **13b** (260 mg, 1 mmol), 3-methoxyaniline (120 mg, 1 mmol) and Et_3N (0.5 mL) in dry dichloromethane (10 mL) was added [1,1'-biphenyl]-4,4'-dicarbonyl dichloride (280 mg, 1 mmol) at 0 ^{o}C. Stirring was continued for 4 h at 0 ^{o}C then the reaction mixture was washed with water (5 mL ×3), and concentrated under reduced pressure. Purification of the residue by chromatography (silica gel, hexane/ethyl acetate = 2/1) gave the product **13c** (240 mg, 42%). To a solution of **13c** (115 mg, 0.2 mmol) in dichloromethane (1 mL) was added trifluoroacetic acid (1 mL) with stirring at room temperature. Stirring was continued for 4 h and all the volatile components were removed under reduced pressure. The resulting residue was purified by chromatography (silica gel, chloroform/MeOH = 5/1) to give the final product **13** (112 mg, 95%). ^{1}H NMR (methanol-d_4, 400 MHz) 8.45 (s, 1H), 8.03 (m, 4H), 7.90-7.80 (m, 6H), 7.59 (m, 2H), 7.30 (m, 1H), 6.71 (m, 1H), 4.09 (s, 4H), 3.78 (s, 3H). HRMS (ESI): m/z $[M + H]^+$ Calcd for $C_{30}H_{27}N_4O_3$, 491.2083; found 491.2084. Purity of the product determined by HPLC (Phenomenex C6-Phenyl 110A. 100×2 mm, 3 μm, 280 nm, retention time = 6.5 min): 97.5%.

N^1,N^4-bis(4-(4,5-dihydro-1*H*-imidazol-2-yl)phenyl)-2-nitroterephthalamide dihydrochloride (14)

The compound was obtained from the Drug Synthesis and Chemistry Branch, Developmental Therapeutics Program, Division of Cancer Treatment and Diagnosis, National Cancer Institute. ^{1}H NMR (methanol-d_4, 400 MHz), 8.78 (d, J = 1.6 Hz, 2H), 8.42 (d, J = 8.0 Hz, 1H), 8.07 (dd, J = 8.8 Hz, 2H), 7.95-7.87 (m, 9H), 4.08 (s, 8H). HPLC-MS: m/z $[M + H]^+$ calculated for $C_{26}H_{24}N_7O_4$, 498.1890; found 498.1882. Purity of the product determined by HPLC (Phenomenex C6-Phenyl 110A. 100×2 mm, 3 μm, 280 nm, retention time = 5.0 min): 95.2%.

(2*S*,3*R*,4*S*,5*S*,6*R*)-2-(3-((4-((3-(4,5-dihydro-1*H*-imidazol-2-yl)phenyl)ethynyl) phenyl)ethynyl)phenoxy)-6-(hydroxymethyl)tetrahydro-2*H*-pyran-3,4,5-triol (15)

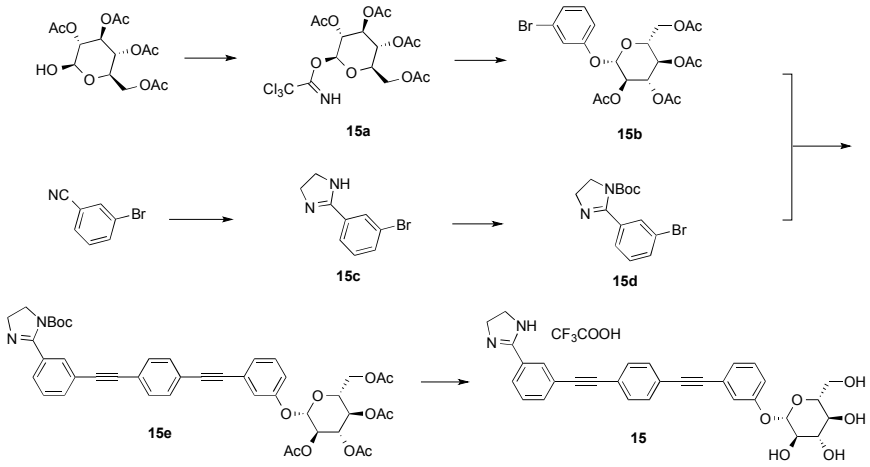

Glucose tetraacetate (3.5 g, 10 mmol) was treated with trichloroacetonitrile (14.4 g, 100 mmol), DBU (0.3 g, 2 mmol) and CH_2Cl_2 (40 mL). The solution was stirred at room temperature for 12 h and then washed with water. The residue was extracted with Et_2O, dried under vacuum and purified by flash chromatography (silica gel, hexane/ethyl acetate = 2/1) to give the peracetyl glucopyranosyl trichloroacetimidate **15a** (4.4 g, 90%). A mixture of **15a** (4.0 g, 8 mmol), 3-bromophenol (1.4 g, 8 mmol), and freshly activated 4 Å molecular sieves in anhydrous CH_2Cl_2 (30 mL) was stirred under N_2 at 0 ^{o}C for 10 min, then BF_3Et_2O (40 μL, 0.8 mmol) was added through a syringe. Stirring continued for 3 h, Et_3N (2 mL) was added, and the resulting mixture

filtered through Celite. The filtrate was concentrated and the residue purified by silica gel column chromatography (hexane/ethyl acetate = 3/1) to give 3-bromophenol glycoside **15b** (3.2 g, 80%). 3-bromobenzonitrile (1.8 g, 10 mmol) was treated with ethylene diamine (20 mL) and NaHS (100 mg). The solution was heated at 110 ^{o}C for 48 h and then quenched with water. The residue was extracted with ethyl acetate, dried under vacuum and purified by flash chromatography (silica gel, hexane/ethyl acetate = 2/1) to give the dihydroimidazole compound **15c** (1.3 g, 60%). To a solution of **15c** (440 mg, 2 mmol) and $NaHCO_3$ (710 mg, 8 mmol) in dichloromethane (6 mL) and water (6 mL) was added $(Boc)_2O$ (900 mg, 4 mmol) with vigorous stirring at 0 ^{o}C. Stirring was continued for 12 h at which point the temperature had risen to room temperature. The dichloromethane phase was separated and concentrated to give the Boc protected product **15d**. To a solution of 1,4-diethynylbenzene (66 mg, 0.5 mmol), **15b** (500 mg, 1.0 mmol) and **15d** (320 mg, 1.0 mmol) in toluene (freshly distilled from sodium, 3 mL) was added CuI (4 mg, 0.03 mmol), $Pd(PPh_3)_4$, then Et_3N (82 μL, 0.5 mmol) under an N_2 atmosphere. Stirring was continued for 4 h at 60 ^{o}C. Purification with flash chromatography (silica gel, hexane/ethyl acetate = 3/1) gave the coupling product **15e** (80 mg, yield: 20%). To a solution of **15e** (80 mg, 0.1 mmol) in MeOH (1 mL) was added MeONa (0.3 g) at room temperature. Stirring was continued for 4 h at room temperature, then all volatile components were removed under reduced pressure. The residue was purified by chromatography (silica gel, ethyl acetate) to give the Boc-protected glycoside. To a solution of the Boc-protected glycoside (64 mg, 0.1 mmol) in dichloromethane (1 mL) was added trifluoroacetic acid (0.2 mL) with stirring at room temperature. Stirring was continued for 4 h then all the volatile components were removed under reduced pressure. The resulting residue was purified by chromatography (silica gel, chloroform/MeOH = 5/1) to give the final product **15** (60 mg, 95%). ^{1}H NMR (methanol-d_4, 400

MHz) 8.03 (s, 1H), 7.90 (d, 1H), 7.81 (d, 1H), 7.66 (m, 1H), 7.55 (s, 4H), 7.33-7.10 (m, 4H), 4.12 (s, 4H), 3.90-3.45 (m, 4H). HRMS (ESI): m/z $[M + H]^+$ Calcd for $C_{31}H_{29}N_2O_6$, 525.2026; found 525.2018. Purity of the product determined by HPLC (Phenomenex C6-Phenyl 110A. 100×2 mm, 3 μm, 250 nm, retention time = 6.1 min): 98.9%.

N^4-(3-(4,5-dihydro-1*H*-imidazol-2-yl)phenyl)-$N^{4'}$-(3-(hexyloxy)phenyl)-[1,1-biphenyl]-4,4–dicarboxamide (16)

Compound **16** was made by using the same protocol as described for **13**. ^{1}H NMR (methanol-d_4, 400 MHz) 8.48 (s, 1H), 8.05 (m, 4H), 7.85 (m, 5H), 7.61 (m, 2H), 7.40 (s, 1H), 7.23 (m, 2H), 6.70 (m, 1H), 4.11 (s, 4H), 3.97 (t, J = 6.0 Hz, 2H), 1.77 (m, 2H), 1.48 (m, 2H), 1.36 (m, 4H), 0.91 (t, J = 6.8 Hz, 3H). HRMS (ESI): m/z $[M + H]^+$ Calcd for $C_{35}H_{37}N_4O_3$, 561.2866; found 561.2875. Purity of the product determined by HPLC (Phenomenex C6-Phenyl 110A. 100×2 mm, 3 μm, 280 nm, retention time = 7.2 min): 97.9%.

N^4-(3-(4,5-dihydro-1*H*-imidazol-2-yl)phenyl)-$N^{4'}$-(3-phenoxyphenyl)biphenyl-4,4'-dicarboxamide (17)

Compound **17** was made by using the same protocol as described for **13**. ^{1}H NMR (methanol-d_4, 400 MHz) 8.47 (d, J = 1.6 Hz, 1H), 8.07 (d, J = 8.4 Hz, 2H), 8.01 (d, J = 8.4 Hz, 2H), 7.90-7.81 (m, 5H), 7.6 (m, 2H), 7.48 (s, 1H), 7.44 (d, J = 12.4 Hz, 1H), 7.37-7.30 (m, 3H), 7.11 (t, J = 7.6 Hz, 1H), 7.03 (s, 1H), 7.01 (s, 1H), 6.77 (t, J = 8.0, 1.2 Hz, 1H), 4.11 (s, 4H). HRMS (ESI): m/z $[M + H]^+$ Calcd for $C_{35}H_{29}N4O_3$, 553.2240; found 553.2249. Purity of the product determined by HPLC (Phenomenex C6-Phenyl 110A. 100×2 mm, 3 μm, 210 nm, retention time = 6.3 min): 99.8%.

2,2'-(5,5'-(1,3-phenylenebis(ethyne-2,1-diyl))bis(3-bromo-5,1-phenylene))diethanamine (18)

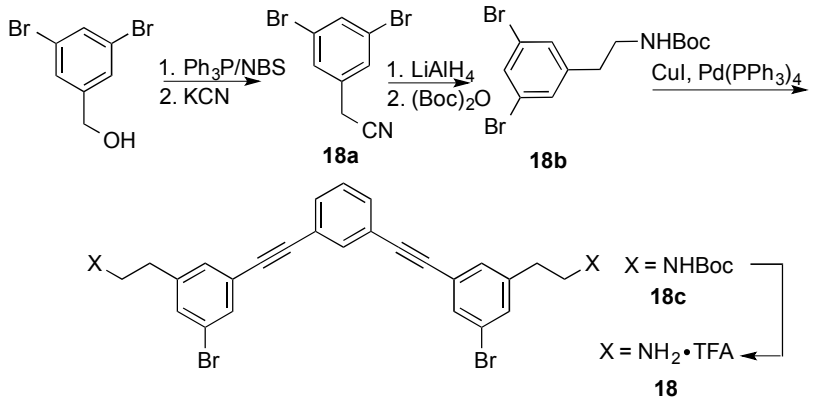

To a solution of 3,5-dibromobenzyl alcohol (1.06 g, 4 mmol) in dichloromethane (15 mL) was added Ph_3P (1.31 g, 5 mmol), then NBS (890 mg, 5 mmol) at 0 ^oC. Stirring was continued for 3 h at 0 ^oC then all volatile components were removed under reduced pressure. Purification with flash chromatography (silica gel, hexane) gave dibromobenzyl bromide (760 mg, yield: 85%). To a solution of dibromobenzyl bromide (700 mg, 2.13 mmol) in DMF (10 mL) was added KCN (277 mg, 4.26 mmol). The mixture was stirred at 80 ^oC for 15 h. The reaction mixture was separated between ethyl acetate and water after it cooled to room temperature. The ethyl acetate phase was evaporated under reduced pressure to give the nitrile product **18a**. To a solution of **18a** in dry Et_2O (10 mL) was added $LiAlH_4$ (74 mg, 2 mmol). The reaction was quenched with NH_4OH (37% in water, 1 mL) after stirring for 2 h at room temperature. The diethyl ether phase was dried over anhydrous Na_2SO_4 then solvent removed under reduced pressure to give the crude amine. To a suspension of the crude amine and $NaHCO_3$ (504 mg, 6 mmol) in a two phase solution (dichloromethane/water, 1/1 v/v, 20 mL) was added $(Boc)_2O$ (872 mg, 4 mmol). Vigorous stirring was continued at room temperature for 12 h. The dichloromethane phase was separated, dried over anhydrous Na_2SO_4, then solvents removed under reduced pressure and the product purified by flash chromatography (silica gel, hexane/ethyl acetate = 10/1) to give the Boc-amine **18b** (411 mg, yield: 51% over 3 steps). To a

solution of 1,3-diethynylbenzene (33 mg, 0.25 mmol) and **18b** (400 mg, 1.1 mmol) in toluene (freshly distilled from sodium, 3 mL) was added CuI (4 mg, 0.03 mmol), $Pd(PPh_3)_4$, then Et_3N (82 μL, 0.5 mmol) under an N_2 atmosphere. Stirring was continued for 4 h at 60 ^oC. Purification with flash chromatography (silica gel, hexane/ethyl acetate, 5/1 v/v) gave product **18c** (63 mg, yield: 35%). 40 mg of **18c** was then added to a 1/1 v/v solution of trifluoroacetic acid/dichloromethane at room temperature. Stirring was continued for 10 min. Purification with flash chromatography (silica gel, chloroform/MeOH, 10/1 v/v) after removing all the volatile components gave the product **18** (26 mg, yield: 62%). ^1H NMR (DMSO-d_6, 500 MHz) δ: 7.66–7.42 (m, 10 H), 3.19(t, J = 8.0 Hz, 4 H), 2.95 (t, J = 8.0 Hz, 4 H) ppm. HRMS (ESI): m/z $[M + H]^+$ calculated for $C_{26}H_{23}Br_2N_2$, 521.0228; found 521.0214. Purity of the product determined by HPLC (Phenomenex C6-Phenyl 110A. 100×2 mm, 3 μm, 280 nm, retention time = 6.4 min): 96.5%.

[1-Hydroxy-2-(3-{3-[3-(2-hydroxy-2,2-bis-phosphono-ethyl)-biphenyl-3-ylsulfamoyl]-benzenesulfonylamino}-biphenyl-3-yl)-1-phosphono -ethyl] -phosphonic acid (19)

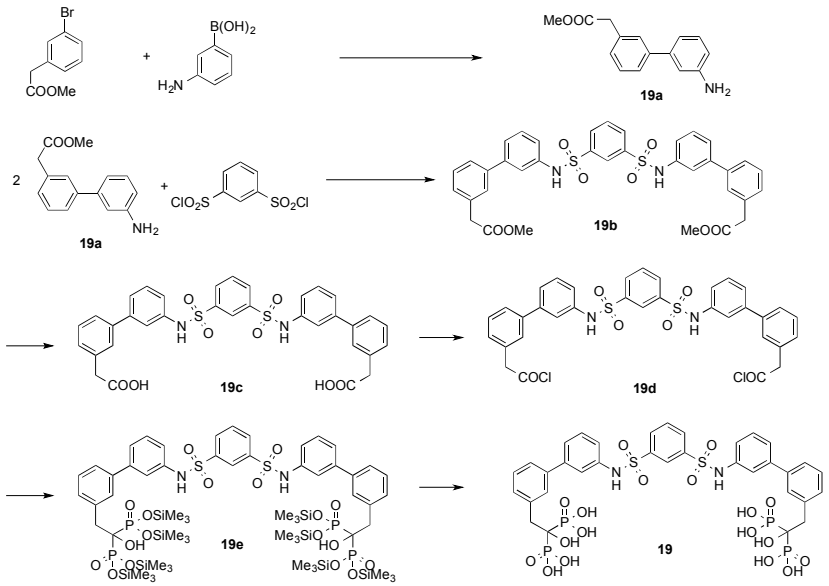

To a solution of methyl 2-(3-bromophenyl) acetate (2.3 g, 10 mmol) and 3-aminophenyl boronic acid (2.1 g, 15 mmol) in toluene was added $Pd(PPh_3)_4$ (260 mg, 1 mmol) and K_2CO_3 (2.8 g, 20 mmol). The solution was heated at 100 ^oC for 24 h then quenched with water. The biphenyl product **19a** was extracted with ethyl acetate (30 mL ×3) and the organic layers combined and solvents removed under vacuum. The residue was purified with flash column chromatography to yield **19a** (1.6 g, 66%). Compound **19a** (1.2 g, 5 mmol) was then treated with benzene-1,3-disulfonyl dichloride (1.5 g, 5.5 mmol) and triethyl amine (2 mL) and CH_2Cl_2 (30 mL) under nitrogen and the solution stirred at room temperature for 12 h followed by washing with water and drying under vacuum to yield **19b** (3.3 g, 95%), which was utilized in next step without further purification. Compound **19b** (1.4 g, 2 mmol) was stirred with LiOH (1 g in 10 mL water) and THF (10 mL) for 4 h and then the solution was neutralized with HCl (6 M). The precipitate was collected with a Buchner funnel and washed with water and acetone. The residue was the crude acid product **19c** (1.3 g, 95%) and was used in next step without further purification. The acid **19c** (1.3 g, 2 mmol) was treated with $(COCl)_2$ (1 mL) in the presence of CH_2Cl_2 (20 mL) and DMF (1 drop). The mixture was stirred under nitrogen at room temperature for 10 h then dried under vacuum to give the acyl chloride **19d** (1.4 g, 99%) which was used in next step without purification. The acyl chloride **19d** (1.4 g, 2 mmol) was treated with tris(trimethylsilyl) phosphate (0.6 g, 4 mmol) and THF (20 mL) and the mixture stirred at room temperature for 1 h to yield intermediate **19e** which was then treated with methanol and stirred at room temperature for 1 h to give the final product **19** (1.2 g, 60%). ^1H NMR (D_2O, 500 MHz) 8.05 (s, 1H), 7.70 (m, 2H), 7.42-6.83 (m, 15H), 6.52 (m, 2H), 3.35 (m, 2H),2.90 (m, 4H). Microchemical analysis (C, H, N): calculated: 38.87% (C), 3.55% (H), 2.67% (N); Found: 38.48% (C), 3.93% (H), 2.9% (N).

Protein Expression, Purification and Inhibition. EcUPPS and SaUPPS were expressed and purified as described previously.[6] UPPS inhibition assays were also carried out as described previously.[6] Briefly, the condensation of FPP with IPP catalyzed by UPPS was monitored by using a continuous spectrophotometric assay[30] in 96 well plates with 200 μL reaction mixtures containing 400 μM MESG, 25 μM IPP, 2.5 μM FPP, 25 μM Tris-HCl (pH 7.5), 0.01% Triton X-100 and 1 mM $MgCl_2$. The IC_{50} values were obtained by fitting the inhibition data to a rectangular hyperbolic dose-response function in GraphPad PRISM 4.0 software (Graphpad Software, San Diego, CA).

Cell Growth Inhibition Assay. The growth of *E. coli* (K12) and determination of EC_{50} values were carried out as described previously.[31] EC_{50} values for *S. aureus* growth inhibition were also determined as described previously.[32] Briefly, an overnight culture of *S. aureus* (Newman strain) was diluted 50-fold into fresh TSB (tryptic soy broth) and grown for 1 h at 37 °C and then diluted 100-fold into fresh TSB medium. 100 μL aliquots were inoculated into each well of a 96-round-bottom culture plate (Corning Inc., Corning, NY) containing serially diluted compounds and plates were incubated for 9 h with shaking, at 37 °C. Absorbances were measured at 600 nm and dose-response curves constructed using GraphPad PRISM 4.0 software (Graphpad Software, San Diego, CA).

Differential Scanning Calorimetry. The DNA dodecamer $(CGCGAATTCGCG)_2$ was purchased from Integrated DNA Technologies, Inc. (Coralville, Iowa). DNA and ligand solutions were prepared in Mes buffer (0.01 M Mes, pH 6.2, 0.001 M EDTA, 0.2 M NaCl). All ligand solutions were prepared by adding appropriate amounts of compound powder into a 0.1 mM DNA solution, the final compound concentrations being 0.1 mM. DSC experiments were performed by using a Microcal VP-DSC instrument. The scans covered the 30 to 110 °C range at

a rate of 90 °C/h. DSC thermograms were analyzed by using Origin 7.1 software (OriginLab Corporation, Northampton, MA). Buffer vs. buffer scans were used for baseline corrections.

X-Ray Crystallography. Native *E. coli* UPPS crystals (prepared as described previously[29]) for use in soaking were obtained by using the hanging-drop method kits from Hampton Research, Laguna Niguel, CA by mixing 2 μL of UPPS solution with 2 μL of mother liquor (20% ethylene glycol and 2-5% PEG 35K) and then equilibrating with 500 μL mother liquor at room temperature. Orthorhombic crystals appeared in 2 days and were then soaked in a cryoprotectant solution (30% ethylene glycol and 5% PEG 35K) containing 5 mM inhibitors, for 3 h. Native *S. aureus* UPPS crystals (*apo*-structure) were obtained by using the hanging-drop method by mixing 2 μL of UPPS solution (25 mM Tris-HCl, pH 7.5 and 150 mM NaCl) with 2 μL of mother liquor (100 mM HEPES, pH 6.5, 200 mM $MgCl_2$, 200 mM $NiCl_2$ and 20% PEG3350) and then equilibrating with 500 μL mother liquor at room temperature. Crystals appeared in 2 days and were then soaked in a cryoprotectant solution (100 mM HEPES, pH 6.5, 200 mM $MgCl_2$, 200 mM $NiCl_2$, 25% PEG3350 and 10% glycerol) for 3 s before data collection. *S. aureus* UPPS crystals with FSPP were obtained by using the hanging-drop method by mixing 1 μL of UPPS solution (~5 mg/ml UPPS in 25 mM Tris-HCl, pH 7.5, 150 mM NaCl, 1.5 mM $MgCl_2$, and 1.5 mM FSPP) with 1 μL of mother liquor (100 mM NaMES, pH 6.5, 200 mM $(NH_4)SO_4$, and 25% PEG MME 5K) and then equilibrating with 400 μL mother liquor at room temperature. Crystals appeared overnight. DNA/ligand complex crystals were obtained via co-crystallization by mixing 0.6 mM dodecamer with the compounds of interest (0.5-5 mM) and left on ice, overnight. These mixtures were then used to grow crystals from hanging drops by mixing 1.5 μL of the mixtures with 1.5 μL of mother liquor (40 mM sodium cacodylate, pH 6.9, 50 mM

$Mg(OAc)_2$ and 6 mM spermine) against a reservoir of 40% MPD. Crystals appeared in about one week.

X-ray diffraction data for *E. coli* UPPS, *S. aureus* UPPS and DNA complexes were collected at the Life Science Collaborative Access Team (LS-CAT) 21-ID-D (G) at the Advanced Photon Source of Argonne National Laboratory, and beamlines 15A1 and 13B1 of the National Synchrotron Radiation Research Center of Taiwan. Diffraction data were processed and scaled by using the program HKL3000 (HKL Research Inc., Charlottesville, VA, USA). Structure refinements were carried out by using Refmac,[33] and Coot.[34] All structure figures were prepared by using PyMOL.[35] Protein/DNA-ligand interactions were calculated by using PDBsum.[36] The statistics for data collection are listed in Tables 2 and 3.

Computational Aspects. All mathematical modeling, heat-map and correlation calculations were performed in R (http://www.R-project.org). Mathematical descriptors were calculated by using MOE.[26]

ASSOCIATED CONTENT

Supporting Information

Supporting Information Available: additional Tables and Figures illustrating statistics for the correlations, ligand electron density maps, protein/DNA-ligand interactions. This material is available free of charge via the Internet at http://pubs.acs.org.

Accession Codes

The atomic coordinates and structure factors (PDB ID codes 4U8A, 4U8B, 4U8C, 4U82, 3WYI, and 3WYJ) have been deposited in the Protein Data Bank, Research Collaboratory for Structural Bioinformatics, Rutgers University, New Brunswick, NJ (http://www.rcsb.org/).

AUTHOR INFORMATION

Corresponding Author

* E-mail: eoldfiel@illinois.edu. Tel: 217-244-0997.

Author Contributions

W.Z. and E.O. designed research; Y.W., K.L. and Y.Z. synthesized compounds; W.Z. performed enzymatic and cell growth inhibition assays and DSC experiments; W.Z., J.G., C.-H.H., C.-C.C., T.-P.K. and R.-T.G. performed crystallographic experiments; W.Z. and E.O. analyzed data. W.Z. and E.O. wrote the paper.

Notes

The authors declare no competing financial interest.

ACKNOWLEDGMENT

This work was supported by the United States Public Health Service (National Institutes of Health grant GM065307); a Harriet A. Harlin Professorship and the University of Illinois/Oldfield Research Fund; the National Basic Research Program of China (grants 2011CB710800 and 2011CBA00805) and the National Natural Science Foundation of China (grants 31200053 and 31300615). We thank Yigui Gao from the University of Illinois Macromolecular Crystallization Laboratory for providing crystallization facilities, and Professor T.E. Kehl-Fie (University of Illinois, Urbana-Champaign) for providing the *S. aureus* Newman strain. We thank the National Synchrotron Radiation Research Center of Taiwan for beam-time allocation and data collection assistance. Use of the Advanced Photon Source was supported by the US Department of Energy, Office of Science, Office of Basic Energy Sciences, under Contract DE-AC02-06CH11357. Use of the Life Science Collaborative Access Team Sector 21 was supported by the Michigan Economic Development Corporation and Michigan Technology Tri-Corridor Grant 085P1000817.

ABBREVIATIONS

UPPS, undecaprenyl diphosphate synthase; FPPS, farnesyl diphosphate synthase; FICI, fractional inhibitory concentration index; FSPP, S-*thiolo* farnesyl diphosphate; MRSA, meticillin-resistant *Staphylococcus aureus*; IC_{50}, half maximal inhibitory concentration; EC_{50}, half maximal effective concentration; SaUPPS, *Staphylococcus aureus* undecaprenyl diphosphate synthase; EcUPPS, *Escherichia coli* undecaprenyl diphosphate synthase; THF, tetrahydrofuran; TSB, tryptic soy broth; MESG, 7-Methyl-6-thioguanosine; IPP, isopentenyl diphosphate; FPP, farnesyl diphosphate; PEG, polyethylene glycol; MME, monomethyl ether; MPD, 2-methyl-2,4-pentanediol.

REFERENCES

(1) Centers for Disease Control and Prevention. Antibiotic resistance threats in the United States, 2013. http://www.cdc.gov/features/AntibioticResistanceThreats/index.html.

(2) World Health Organization. Antimicrobial resistance: global report on surveillance, 2014. http://www.who.int/drugresistance/documents/surveillancereport/en/.

(3) Davies, S.; Grant, J.; Catchpole, M. The drugs don't work: a global threat. Penguin Books Ltd, 2013.

(4) Durrant, J. D.; Cao, R.; Gorfe, A. A.; Zhu, W.; Li, J.; Sankovsky, A.; Oldfield, E.; McCammon, J. A. Non-bisphosphonate inhibitors of isoprenoid biosynthesis identified via computer-aided drug design. *Chem. Bio. Drug Design* **2011**, *78*, 323-332.

(5) Lindert, S.; Zhu, W.; Liu, Y. L.; Pang, R.; Oldfield, E.; McCammon, J. A. Farnesyl diphosphate synthase inhibitors from *in silico* screening. *Chem. Bio. Drug Design* **2013**, *81*, 742-748.

(6) Zhu, W.; Zhang, Y.; Sinko, W.; Hensler, M. E.; Olson, J.; Molohon, K. J.; Lindert, S.; Cao, R.; Li, K.; Wang, K.; Wang, Y.; Liu, Y. L.; Sankovsky, A.; de Oliveira, C. A.; Mitchell, D. A.; Nizet, V.; McCammon, J. A.; Oldfield, E. Antibacterial drug leads targeting isoprenoid biosynthesis. *Proc. Natl. Acad. Sci. USA* **2013**, *110*, 123-128.

(7) Ashley, J. N.; Barber, H. J.; Ewins, A. J.; Newbery, G.; Self, A. D. H. A chemotherapeutic comparison of the trypanocidal action of some aromatic diamidines. *J. Chem. Soc.* **1942**, 103-116.

(8) Fischer, R.; Hirt, R. Carbanilide compounds. US Patent No. 3,622,596, 1971.

(9) Williams, J. D.; Nguyen, S. T.; Gu, S.; Ding, X. Y.; Butler, M. M.; Tashjian, T. F.; Opperman, T. J.; Panchal, R. G.; Bavari, S.; Peet, N. P.; Moir, D. T.; Bowlin, T. L. Potent and

broad-spectrum antibacterial activity of indole-based bisamidine antibiotics: synthesis and SAR of novel analogs of MBX 1066 and MBX 1090. *Bioorgan. Med. Chem.* **2013**, *21*, 7790-7806.

(10) Steverding, D. The development of drugs for treatment of sleeping sickness: a historical review. *Parasites & Vectors* **2010**, *3*, 15.

(11) Panchal, R. G.; Ulrich, R. L.; Lane, D.; Butler, M. M.; Houseweart, C.; Opperman, T.; Williams, J. D.; Peet, N. P.; Moir, D. T.; Nguyen, T.; Gussio, R.; Bowlin, T.; Bavari, S. Novel broad-spectrum bis-(imidazolinylindole) derivatives with potent antibacterial activities against antibiotic-resistant strains. *Antimicrob. Agents Chemother.* **2009**, *53*, 4283-4291.

(12) Butler, M. M.; Williams, J. D.; Peet, N. P.; Moir, D. T.; Panchal, R. G.; Bavari, S.; Shinabarger, D. L.; Bowlin, T. L. Comparative *in vitro* activity profiles of novel bis-indole antibacterials against gram-positive and gram-negative clinical isolates. *Antimicrob. Agents Chemother.* **2010**, *54*, 3974-3977.

(13) T.J. Opperman, C. H., D. Aiello, J.D. Williams, N.P. Peet, D.T. Moir, T.L. Bowlin. Poster Seesion, 50th Interscience Conference on Antimicrobial Agents and Chemotherapy, Boston, September 12-15, 2010.

(14) Lanteri, C. A.; Trumpower, B. L.; Tidwell, R. R.; Meshnick, S. R. DB75, a novel trypanocidal agent, disrupts mitochondrial function in *Saccharomyces cerevisiae*. *Antimicrob. Agents Chemother.* **2004**, *48*, 3968-3974.

(15) Oldfield, E.; Feng, X. Resistance-resistant antibiotics. *Trends in Pharmacol. Sci.* **2014**. doi:10.1016/j.tips.2014.10.007

(16) Silver, L. L. Challenges of antibacterial discovery. *Clin. Microb. Rev.* **2011**, *24*, 71-109.

(17) Wilson, W. D.; Tanious, F. A.; Mathis, A.; Tevis, D.; Hall, J. E.; Boykin, D. W. Antiparasitic compounds that target DNA. *Biochimie* **2008**, *90*, 999-1014.

(18) Chai, Y.; Paul, A.; Rettig, M.; Wilson, W. D.; Boykin, D. W. Design and synthesis of heterocyclic cations for specific DNA recognition: from AT-rich to mixed-base-pair DNA sequences. *J. Org. Chem.* **2014**, *79*, 852-866.

(19) Barrett, M. P.; Gemmell, C. G.; Suckling, C. J. Minor groove binders as anti-infective agents. *Pharmacol. Ther.* **2013**, *139*, 12-23.

(20) Scott, R. W.; DeGrado, W. F.; Tew, G. N. *De novo* designed synthetic mimics of antimicrobial peptides. *Curr. Opin. Biotechnol.* **2008**, *19*, 620-627.

(21) Leon, A.; Liu, L.; Yang, Y.; Hudock, M. P.; Hall, P.; Yin, F. L.; Studer, D.; Puan, K. J.; Morita, C. T.; Oldfield, E. Isoprenoid biosynthesis as a drug target: Bisphosphonate inhibition of *Escherichia coli* K12 growth and synergistic effects of fosmidomycin. *J. Med. Chem.* **2006**, *49*, 7331-7341.

(22) Teng, M. K.; Usman, N.; Frederick, C. A.; Wang, A. H. The molecular structure of the complex of Hoechst 33258 and the DNA dodecamer d(CGCGAATTCGCG). *Nuc. Acids Res.* **1988**, *16*, 2671-2690.

(23) Nunn, C. M.; Jenkins, T. C.; Neidle, S. Crystal structure of d(CGCGAATTCGCG) complexed with propamidine, a short-chain homologue of the drug pentamidine. *Biochem.* **1993**, *32*, 13838-13843.

(24) Squire, C. J.; Clark, G. R.; Denny, W. A. Minor groove binding of a bis-quaternary ammonium compound: the crystal structure of SN 7167 bound to $d(CGCGAATTCGCG)_2$. *Nuc. Acids Res.* **1997**, *25*, 4072-4078.

(25) Mukkamala, D.; No, J. H.; Cass, L. M.; Chang, T. K.; Oldfield, E. Bisphosphonate inhibition of a Plasmodium farnesyl diphosphate synthase and a general method for predicting cell-based activity from enzyme data. *J. Med. Chem.* **2008**, *51*, 7827-7833.

(26) Molecular Operating Environment (MOE), 2013.08; Chemical Computing Group Inc., 1010 Sherbooke St. West, Suite #910, Montreal, QC, Canada, H3A 2R7, 2014.

(27) Ammirati, M.; Pandit, J. Crystal structure of *Staphylococcus* undecaprenyl pyrophosphate synthase and uses thereof. US Patent Application No. 10/688,167, 2002.

(28) Altschul, S. F.; Madden, T. L.; Schaffer, A. A.; Zhang, J.; Zhang, Z.; Miller, W.; Lipman, D. J. Gapped BLAST and PSI-BLAST: a new generation of protein database search programs. *Nuc. Acids Res.* **1997**, *25*, 3389-3402.

(29) Guo, R. T.; Cao, R.; Liang, P. H.; Ko, T. P.; Chang, T. H.; Hudock, M. P.; Jeng, W. Y.; Chen, C. K.; Zhang, Y.; Song, Y.; Kuo, C. J.; Yin, F.; Oldfield, E.; Wang, A. H. Bisphosphonates target multiple sites in both *cis*- and *trans*-prenyltransferases. *Proc. Natl. Acad. Sci. USA* **2007**, *104*, 10022-10027.

(30) Webb, M. R. A continuous spectrophotometric assay for inorganic phosphate and for measuring phosphate release kinetics in biological systems. *Proc. Natl. Acad. Sci. USA* **1992**, *89*, 4884-4887.

(31) Li, K.; Schurig-Briccio, L. A.; Feng, X. X.; Upadhyay, A.; Pujari, V.; Lechartier, B.; Fontes, F. L.; Yang, H. L.; Rao, G. D.; Zhu, W.; Gulati, A.; No, J. H.; Cintra, G.; Bogue, S.; Liu, Y. L.; Molohon, K.; Orlean, P.; Mitchell, D. A.; Freitas-Junior, L.; Ren, F. F.; Sun, H.; Jiang, T.; Li, Y. J.; Guo, R. T.; Cole, S. T.; Gennis, R. B.; Crick, D. C.; Oldfield, E. Multitarget drug discovery for tuberculosis and other infectious diseases. *J. Med. Chem.* **2014**, *57*, 3126-3139.

(32) Kehl-Fie, T. E.; Zhang, Y.; Moore, J. L.; Farrand, A. J.; Hood, M. I.; Rathi, S.; Chazin, W. J.; Caprioli, R. M.; Skaar, E. P. MntABC and MntH contribute to systemic *Staphylococcus aureus* infection by competing with calprotectin for nutrient manganese. *Infec. Immun.* **2013**, *81*, 3395-3405.

(33) Potterton, E.; Briggs, P.; Turkenburg, M.; Dodson, E. A graphical user interface to the CCP4 program suite. *Acta Cryst. Sect. D, Biol. Cryst.* **2003**, *59*, 1131-1137.

(34) Emsley, P.; Cowtan, K. Coot: model-building tools for molecular graphics. *Acta Cryst. Sect. D, Biol. Cryst.* **2004**, *60*, 2126-2132.

(35) The PyMOL Molecular Graphics System, Version 1.5.0.4. Schrödinger, LLC.

(36) de Beer, T. A.; Berka, K.; Thornton, J. M.; Laskowski, R. A. PDBsum additions. *Nuc. Acids res.* **2014**, *42*, D292-296.

Table of Contents graphic